applied sciences

MDPI

Article

Carbenoxolone as a Multifunctional Vehicle for Electrodeposition of Materials

Xinqian Liu [1], Stephen Veldhuis [2], Ritch Mathews [3] and Igor Zhitomirsky [1,*]

[1] Department of Materials Science and Engineering, McMaster University, Hamilton, ON L8S 4L7, Canada; liux234@mcmaster.ca
[2] Department of Mechanical Engineering, McMaster University, Hamilton, ON L8S 4L7, Canada; veldhu@mcmaster.ca
[3] Advanced Ceramics Corporation, 2536 Bristol Circle, Oakville, ON L6H 5S1, Canada; rmathews@acc.ca
* Correspondence: zhitom@mcmaster.ca

Abstract: This investigation describes for the first time the application of carbenoxolone for electrophoretic deposition (EPD) of different carbon materials, polytetrafluoroethylene (PTFE) and their composite films. Carbenoxolone is a versatile biosurfactant, which adsorbs on materials due to its amphiphilic structure and allows their charging and dispersion. Moreover, carbenoxolone exhibits film-forming properties, which are investigated in experiments on EPD of films using water and ethanol-water solvents. The new deposition process is monitored in situ and the deposition yield and film microstructure are analyzed at different conditions. The EPD mechanism of materials involves electrode reactions of the carbenoxolone surfactant. The data of potentiodynamic studies coupled with the results of impedance spectroscopy show that PTFE films can be applied to protect metals from corrosion. Electron microscopy, electrochemical techniques and modeling are used for analysis of the microstructure and porosity of films prepared at different conditions. Carbenoxolone is applied as a co-surfactant for the EPD of composites.

Keywords: electrophoretic deposition; film; diamond; polytetrafluoroethylene; graphene; composite; dispersant; corrosion protection

Citation: Liu, X.; Veldhuis, S.; Mathews, R.; Zhitomirsky, I. Carbenoxolone as a Multifunctional Vehicle for Electrodeposition of Materials. *Appl. Sci.* **2021**, *11*, 9110. https://doi.org/10.3390/app11199110

Academic Editor: Valentina Belova

Received: 31 August 2021
Accepted: 27 September 2021
Published: 30 September 2021

1. Introduction

EPD and other electrochemical strategies are widely applied to modify the surfaces of materials and to form coatings and thin films [1–6]. The EPD technique involves electrophoresis of charged particles and their deposition on the electrode surface [7–10]. Many investigations have been conducted to develop surface engineering strategies to charge particles and to develop deposition mechanisms and optimize the deposition conditions [11–14]. Advanced techniques, novel additives and bath compositions have been applied for EPD [15–17]. There has been significant progress in the EPD of composite and multilayer films [18–21]. EPD was combined with electrosynthesis for the manufacturing of nanocomposite organic–inorganic films [22,23]. A new approach involved the use of film-forming charged dispersants for EPD of materials [24,25]. It was found that small organic molecules such as bile salts adsorbed on carbon nanotubes and the negative charge of the adsorbed molecules facilitated carbon nanotube dispersion [24]. Moreover, bile salts exhibited both a pH-dependent charge and gel properties, which facilitated the fabrication of thin films of bile acids [24]. The film-forming and binding properties of bile salts facilitated EPD of materials. Therefore, further development of film-forming charged dispersants is a promising approach to surface modification and EPD of materials.

EPD is an eco-friendly technology which facilitates the deposition of thin films of different functional materials, avoiding the use of toxic precursors and solvents [26]. It is widely used for high quality film deposition for various electronic and biomedical applications due to the high purity of the deposited materials [26,27]. One of the challenges

in designing EPD processes is the development of eco-friendly charged surfactants for various materials. Therefore, the use of natural and biocompatible surfactants for charging and dispersion of materials is of particular interest for the development of EPD technology.

Carbenoxolone sodium salt ($CBXNa_2$) is a promising biocompatible molecule which can potentially be used for surface modification and EPD of materials [28]. This molecule was used as an anionic dopant for electropolymerization of polypyrrole [28]. $CBXNa_2$ is currently used in medicine for the treatment of gastric and duodenal ulcers. This drug molecule exhibits important antiviral and gel-forming properties. $CBXNa_2$ is a derivative of glycyrrhetinic acid (Figure 1A) with a steroid-like chemical structure. It is a bipolar amphiphilic molecule, containing carboxylic and succinyl groups bonded to opposite sides of the steroid-like core. Dissociated $CBXNa_2$ exhibits anionic properties in aqueous solutions due to its two COO^- groups. The COO^- groups are protonated in acidic solutions to form insoluble $CBXH_2$. Compared to bile salts, $CBXNa_2$ offers the benefit of a higher charge to mass ratio, which is important for electrostatic dispersion of materials. Another advantage of $CBXNa_2$ is that the succinyl group of $CBXNa_2$ facilitates its bonding to various materials [29].

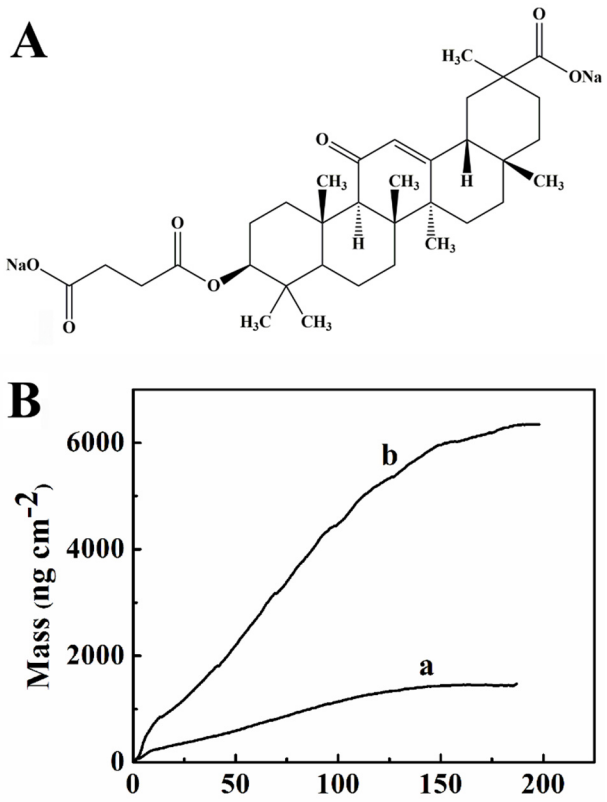

Figure 1. (**A**) $CBXNa_2$ structure, (**B**) film mass as a function of time analyzed in situ using QCM for 0.1 gL^{-1} $CBXNa_2$ solutions in water at deposition voltages of (a) 3 and (b) 5 V.

The goal of this study was the development of a new and versatile approach for EPD of different materials, such as carbon materials, PTFE and composites. It involved the application of $CBXNa_2$ as a versatile surface modification, dispersion, charging and film-forming agent. We analyzed the deposition mechanisms, film microstructures and properties.

2. Materials and Methods

$CBXNa_2$, diamond (size < 1 μm), nanodiamond (size < 10 nm), graphene nanoplatelets (BET area 750 m^2g^{-1}, size < 2 μm) and PTFE (~1 μm) (Aldrich) were used. Carbon dots were prepared as described in [30]. $CBXNa_2$ solutions in water or water-ethanol solvents with dispersed particles of the carbon materials and PTFE were prepared for EPD. The particle concentration was 0.1–10 gL^{-1}, deposition voltages were 3–70 V, deposition times

were 3–5 min. The distance between stainless steel (type 304) and counterelectrodes (Pt foil) in the EPD cell was 15 mm. The electrode dimensions were 25 × 30 × 0.1 mm. PTFE coated samples were annealed at 350 °C for 1 h. The yield of EPD has been analyzed in situ using a microbalance (AMETEK, QCM 922) and Au coated quartz crystals. The area of the electrode was 0.18 cm^2.

Corrosion protection of the electrophoretically deposited films was studied in 3% (mass per volume) sodium chloride solutions using a potentiostat (AMETEK 2273) and a three-electrode cell with uncoated or coated substrate, Pt auxiliary electrode and an SCE reference. The working electrode area was 1 cm^2. Potentiodynamic testing was carried out at a 60 $mVmin^{-1}$ scan rate in the potential range of −1.1–+0.8 V versus SCE. EIS data was acquired at a 5 mV voltage amplitude in the frequency range of 10 mHz–10 kHz. Microstructure studies were carried out using a JSM-7000F microscope (JEOL, SEM) at voltages 5–10 kV. XRD testing was carried out with a Nicolet I2 diffractometer and CuKα radiation. A Bruker FTIR spectrometer (Vertex 70) was applied for spectroscopy analysis using the attenuated total reflection (ATR) technique.

3. Results

A typical requirement for EPD is the colloidal stability of charged species in the deposition bath. The charging agent selection plays an essential role in the control of bath stability and the rate of electrophoresis. However, strong repulsion of charged particles inhibits film formation. Therefore, when selecting charging surface agents for EPD it is important to consider not only bulk suspension stability but also the ability of the agents to facilitate particle discharge and coagulation at the substrate surface. Our strategy is based on the charging of particles by CBX^{2-} species in $CBXNa_2$ solutions and their discharge in electrode reactions.

The ability to form films from pure $CBXNa_2$ solutions is a favorable factor for EPD of materials. The deposition mechanism involved electrolysis of water in an anodic reaction [24,25,31,32]:

$$2H_2O \rightarrow O_2 + 2H^+ + 2e^- \quad (1)$$

The electromigration of CBX^{2-} species led to their discharge at the anode and formation of $CBXH_2$ films:

$$CBX^{2-} + 2H^+ \rightarrow CBXH_2 \quad (2)$$

Reaction (2) is critical for the deposition process, because it results in the discharge of CBX^{2-} and deposition of insoluble $CBXH_2$. The deposition mechanism described in Reactions (1) and (2) is similar to that used for anodic deposition of other small organic molecules and macromolecules [24,25,33,34].

Water is an important component of an electrodeposition bath because it is necessary for the H^+ generation in Reaction (1). However, organic solvents offer several benefits for EPD of materials. The EPD yield is proportional to the electric field in the suspension [35]. The generation of high electric fields in aqueous suspensions by the application of high voltages presents difficulties due to the high conductivity of aqueous suspensions, which results in high currents, significant O_2 gas evolution and enhanced H^+ generation in Reaction (1). The high rate of H^+ generation can result in expansion of a low pH region away from the anode. This can potentially lead to the precipitation of $CBXH_2$ at some distance from the electrode surface. Moreover, significant O_2 evolution results in porous films. The use of ethanol-water mixture as a solvent is beneficial for EPD at relatively high voltages and a reduced rate of Reaction (1). The dispersion of hydrophobic PTFE in water presented difficulties. However, PTFE suspensions were formed in an ethanol-water mixture.

The deposition of pure $CBXH_2$ films was studied using water and ethanol-water (5% water) solvents. The deposition yield was analyzed by in situ method, based on continuous QCM monitoring of deposit mass during the deposition. This technique has limitations, because it can be used for relatively low deposition yields. Therefore, QCM analysis was

performed at relatively low voltages and low solution concentrations. The deposition yield data presented in Figure 1B showed continuous mass increase with time due to film growth. The increase in the applied voltage led to a higher rate of deposition. The rate of mass gain reduced with EPD time due to the continuous rise of the voltage drop in the deposit and reduction of electric field strength in the solution [35].

EPD from aqueous $CBXNa_2$ solutions at voltages below 15V led to the formation of continuous films which were crack-free (Figure 2A,B). However, the deposition at higher voltages resulted in the formation of pinholes, due to the O_2 evolution. In contrast, significantly higher voltages can be applied for the EPD of films from the solutions of $CBXNa_2$ in the ethanol-water mixture. The EPD process resulted in the formation of continuous films at voltages of 20–80 V. The microstructure of the films formed at 20 V showed a large number of fibers with a typical length of 5–10 μm and diameters of about 0.5 μm. Fiber formation can result from self-assembly of water-insoluble hydrophobic $CBXH_2$ molecules. The formation of fibrous particles by electrochemical self-assembly was observed in other experiments on anodic electrodeposition of other small organic molecules [36,37]. Such fibers were not observed at higher voltages. The increase of voltage above 80V in the water-ethanol solvent resulted in pinholes. Therefore, the EPD from aqueous suspensions was limited to voltages not higher than 15 V, whereas the deposition from ethanol-water suspensions was performed at voltages below 80 V. It is important to note that the selection of a solvent is important for the fabrication of stable suspensions for EPD. Therefore, in this investigation EPD of different materials was performed in aqueous or ethanol-water suspensions in order to achieve good suspension stability for each material.

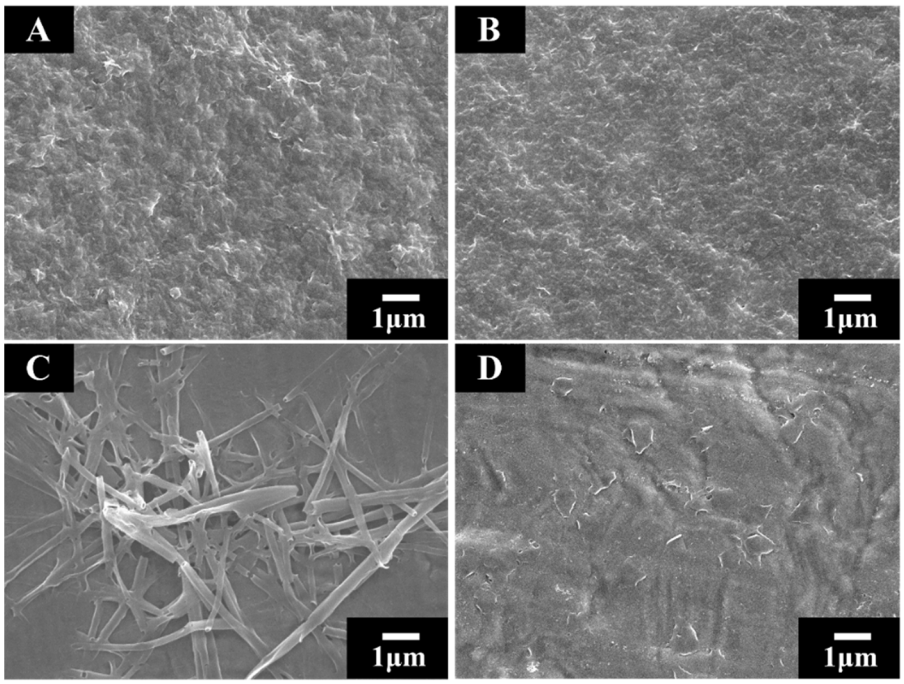

Figure 2. SEM images of films, deposited from 1 g L^{-1} $CBXNa_2$ solutions in water at (**A**) 5 V, (**B**) 15 V and in ethanol-water solvent (5% water) at (**C**) 20 V and (**D**) 80 V.

The deposition mechanism of carbon materials and PTFE involved CBX^{2-} adsorption; the adsorbed CBX^{2-} makes the materials negatively charged and facilitates EPD from stable suspensions. Figure 3 shows microstructures of films containing diamond and nanodiamond, as well as the XRD patterns of the films. Electron microscopy showed the formation of continuous films, which were crack-free and contained diamonds (Figure 3A). Nanodiamond particles showed poor dispersion in water. However, relatively stable suspensions were obtained in ethanol-water solvent, which facilitated nanodiamond dispersion in the

presence of $CBXNa_2$. Electron microscopy studies showed some agglomerates on the film surface (Figure 3B). The size of the primary particles in such agglomerates was significantly larger than the size of the nanodiamond particles. The agglomeration of the nanodiamond particles can result from their lower zeta-potential (Supplementary material, Table S1). The incorporation of diamond and nanodiamond in the films was confirmed by XRD (Figure 3C), which showed peaks (111), (220) and (113) of diamond. The peak broadening for nanodiamond resulted from its small size (Figure 3C).

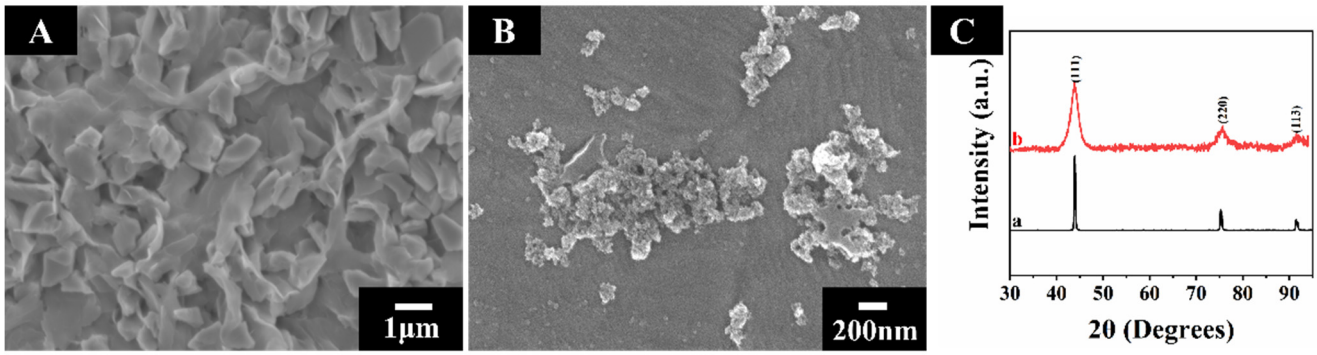

Figure 3. (**A**,**B**) SEM and (**C**) XRD data for films prepared from 1 gL^{-1} $CBXNa_2$ solutions with (**A**,**C**(a)) 1 gL^{-1} diamond at 7 V in water and (**B**,**C**(b)) 1 gL^{-1} nanodiamond at 70 V in ethanol-water (5% water) solvent.

The feasibility of diamond deposition by EPD from their dispersion in $CBXNa_2$ solutions indicated that CBX^{2-} adsorbed on chemically inert diamond surfaces. It was hypothesized that the hydrophobic interactions allowed for adsorption of amphiphilic CBX^{2-} on the diamond particles. It was found that other carbon materials, such as carbon dots and graphene, can also be deposited from their dispersions in the $CBXNa_2$ solutions. Figure 4 shows that continuous and crack-free films were deposited. The SEM image shows relatively large graphene particles. The incorporation of carbon dots into the $CBXH_2$ films was verified by FTIR.

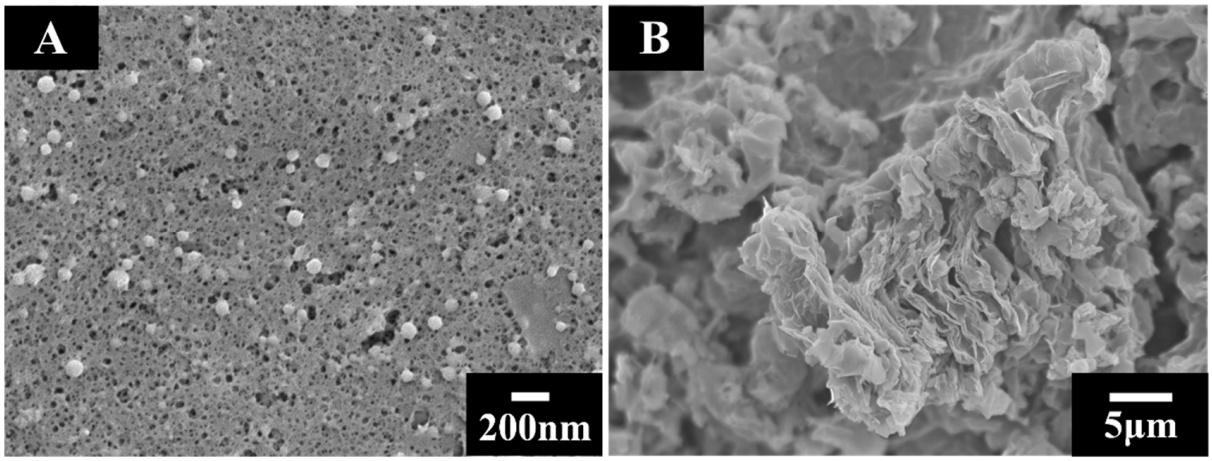

Figure 4. SEM images of films, prepared from (**A**) 0.5 gL^{-1} $CBXNa_2$ with 0.5 gL^{-1} carbon dots in water at 15 V and (**B**) 1 gL^{-1} $CBXNa_2$ with 1 gL^{-1} graphene in water at 10 V.

The FTIR spectrum of $CBXNa_2$ (Figure 5A(a)) presents peaks at 1397 and 1564 cm^{-1}, owing to symmetric and asymmetric vibrating of salified carboxylic groups, respectively [38]. Such absorptions were not observed for the deposited $CBXH_2$ (Figure 5A(b)), which exhibited enhanced absorption at 1716 cm^{-1} due to stretching of the protonated COOH ligand [38]. The peaks at 1647 cm^{-1} (Figure 5A(a)) and 1650 cm^{-1} (Figure 5A(b)) resulted from C=C stretching [39]. Carbon dots (Figure 5A(c)) showed absorptions at 1457 cm^{-1}, attributed to stretching of a C-C type. The minimum, at 1368 cm^{-1}, was observed due to bending of surface C-OH groups [39]. Similar peaks were recorded for the films formed from carbon dot suspensions (Figure 5A(d)).

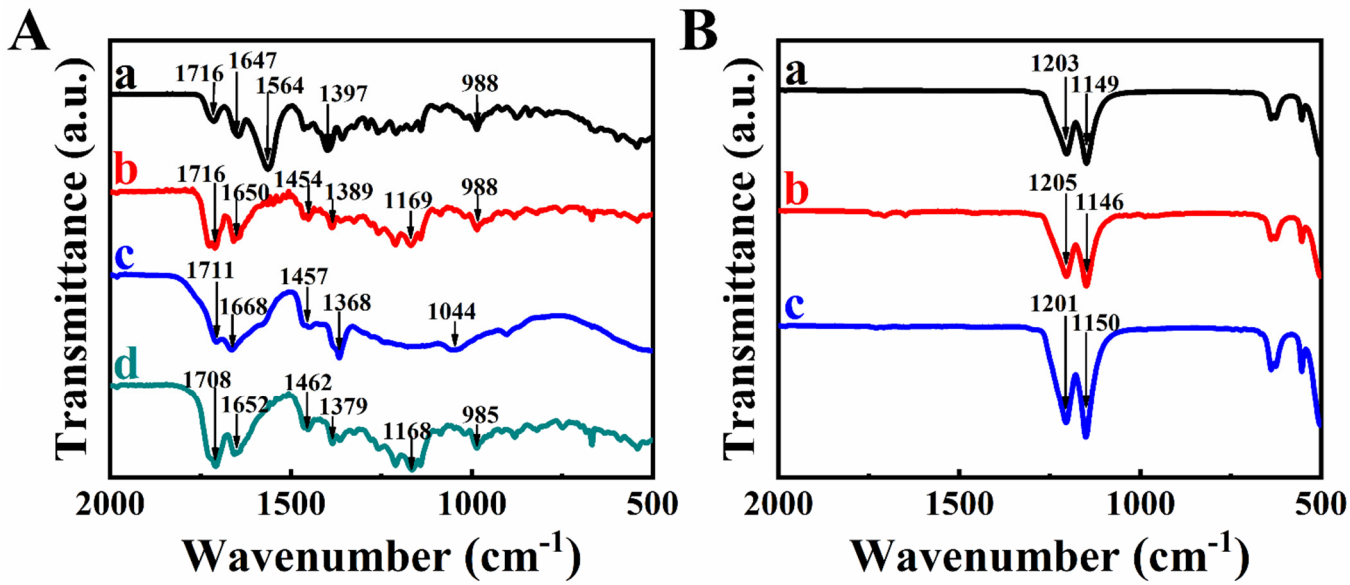

Figure 5. FTIR testing data for (**A**) (a) original $CBXNa_2$, (b) film material, formed from 1gL^{-1} $CBXNa_2$ in water at 15 V, (c) carbon dots, (d) deposit formed from 0.5 gL^{-1} $CBXNa_2$ with 0.5 gL^{-1} carbon dots in water at 15 V; (**B**) (a) PTFE (b,c) deposits, obtained from 1 gL^{-1} $CBXNa_2$ with (b) 0.5 gL^{-1} and (c) 1 gL^{-1} PTFE in ethanol-water solvent at 50 V.

EPD of PTFE was performed from suspension of PTFE particles, which were dispersed and charged using CBX^{2-}. Figure 5B(a) shows FTIR data for PTFE, which exhibits absorptions at 1149 and 1203 cm^{-1}. According to the literature, C–C and C–F_2 asymmetric vibrating contribute to absorption at 1149 cm^{-1}, whereas the minimum at 1203 cm^{-1} was due to symmetric vibrating of C–F_2 [40]. The FTIR spectra of deposits prepared from $CBXNa_2$ solutions (Figure 5B(b,c) containing PTFE showed similar peaks, and confirm the deposition of PTFE.

The higher polymer content in the suspension led to the enlarged polymer content in the film. The electron microscopy imaging data (Figure 6) for the composite deposit formed by EPD from 10 gL^{-1} PTFE suspension contained larger number of the PTFE particles, compared to the film formed from the 5 gL^{-1} PTFE bath. The SEM analysis revealed the formation of continuous deposits. The SEM images for the films prepared from 10 gL^{-1} PTFE suspension showed reduced porosity and relatively dense packing of the submicrometre PTFE particles. Annealing led to the burning out of the $CBXH_2$ phase and melting of the PTFE particles, which resulted in reduced porosity. The films prepared from 5 gL^{-1} PTFE suspension were porous (Figure 6) due to low PTFE content. The increase in the PTFE content in the films resulted in reduced porosity, as indicated by the electron microscopy images of films formed from 10 gL^{-1} PTFE suspensions (Figure 6). Such films were analyzed by potentiodynamic and EIS studies in the 3% NaCl solutions.

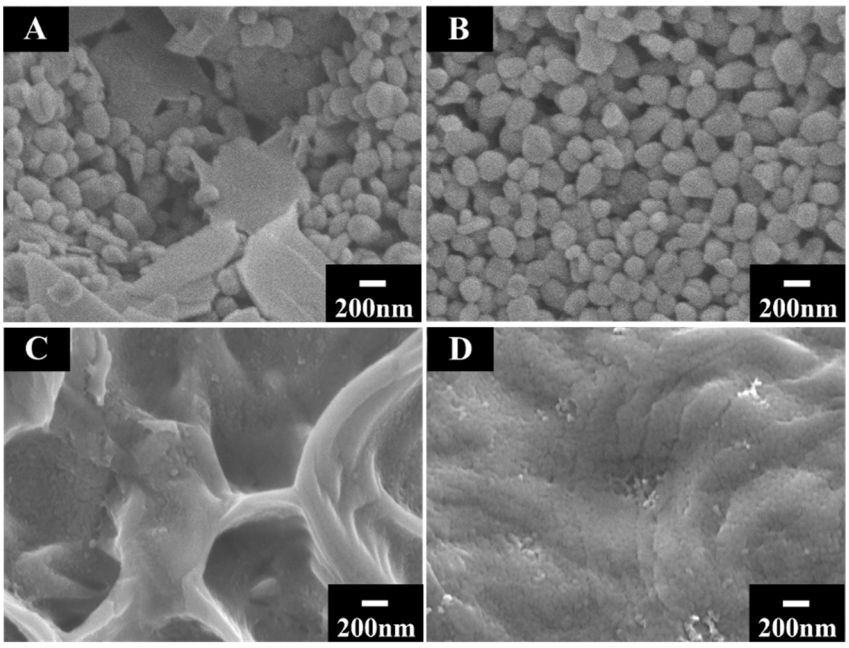

Figure 6. SEM data for films (**A**,**B**) before and (**C**,**D**) after annealing (1 h at 350 °C), for films prepared using 1 gL^{-1} $CBXNa_2$ with (**A**,**C**) 5 gL^{-1} PTFE and (**B**,**D**) 10 gL^{-1} PTFE in ethanol-water solvent at 50 V.

The data from electrochemical testing presented in Figure 7 demonstrate that films of the PTFE polymer allowed for corrosion protection. The Tafel graphs show that coating deposition resulted in a lower current for the anodic part of the graph, with an enlarged corrosion potential. The analysis of the Tafel plots showed corrosion currents of 0.01 and 2.6 μAcm^{-2} for coated and uncoated substrates, respectively. The EIS data presented in the Nyquist plot were analyzed using an equivalent circuit (Figure 7), similar to that described in [41], where R_s, R_{pore} and R_{ct} are solution resistance, resistance of electrolyte in pores and charge transfer resistance, respectively. C_1 represents capacitance of the film and C_2 is a double layer capacitance at the substrate surface in pores. The modeling results correlated with the experimental data.

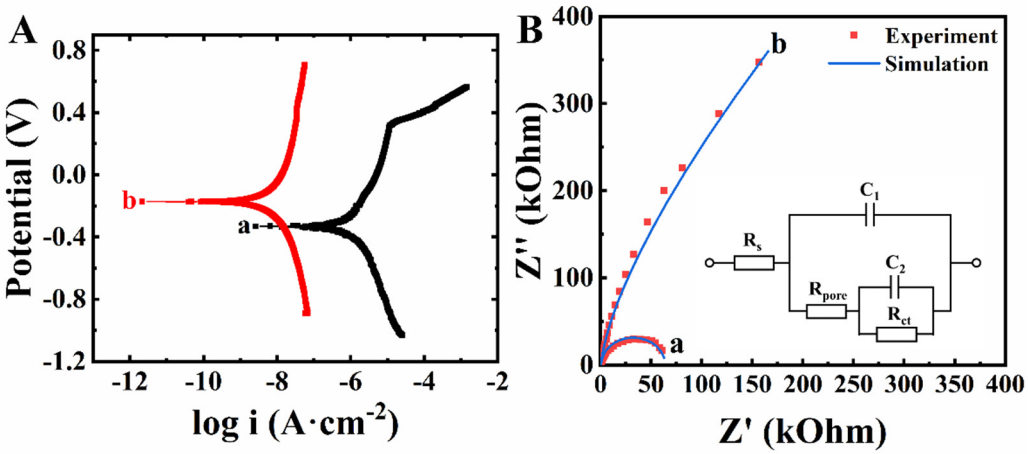

Figure 7. (**A**) Tafel plot, (**B**) Nyquist plot for substrate (a) without and (b) with coating; inset shows equivalent circuit. The working electrode area was 1 cm^2. The coating was deposited from 1 gL^{-1} $CBXNa_2$ with 10 gL^{-1} PTFE in a mixed ethanol-water solvent at 50 V and annealed (1 h at 350 °C).

The porosity (P) of the films was tested according to ref. [41] by the equation

$$P = \frac{R_{pm}}{R_p} \times 10^{-|\Delta E/\beta|} \quad (3)$$

where ΔE is the difference of corrosion potentials for the substrates with and without films, β and R_{pm} are the slope of the anodic part of the Tafel graph and the substrate polarization resistance, respectively, R_p is the polarization resistance of the coated substrate, and $R_p = R_{pore} + R_{ct}$. The EIS data was analyzed with the aid of a circuit (Figure 7) [41], which allowed for measurement of R_{pm} and R_p. The film porosity was found to be 0.28%.

In this investigation the possibility of EPD of PTFE composites has been studied using $CBXNa_2$ as a co-dispersant. Figure 8 presents electron microscopy data for the composite coatings prepared from mixed PTFE and diamond suspensions. The SEM images show relatively dense packing of the PTFE and diamond particles. The electron microscopy images showed that the higher concentration of diamond in the suspension led to a larger diamond content in the films. The films deposited from 1 gL^{-1} $CBXNa_2$ solutions with 5 gL^{-1} PTFE and 0.5 gL^{-1} diamond show individual diamond particles incorporated in the relatively dense PTFE layer. The higher diamond concentration in the EPD bath resulted in films which mainly contained diamond, with PTFE acting as a binder for the diamond particles (Figure 8). The results of the microscopy indicated that the composition of the films can be controlled and varied.

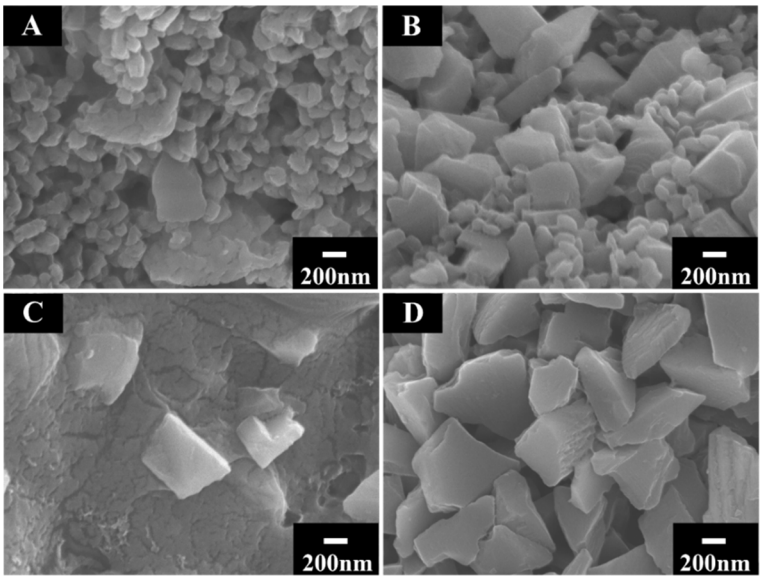

Figure 8. SEM data for films (**A**,**B**) before and (**C**,**D**) after annealing (1 h at 350 °C), for films prepared from 1 gL^{-1} $CBXNa_2$ solutions with 5 gL^{-1} PTFE with (**A**,**C**) 0.5 gL^{-1} and (**B**,**D**) 1 gL^{-1} diamond at 50 V.

The fabrication of continuous $CBXH_2$ films provided evidence of the film-forming properties of $CBXNa_2$. It can also be used as a charging and dispersing agent for particles with functional properties. The combination of film-forming, charging and dispersing properties makes $CBXNa_2$ a promising additive for EPD of materials. The results of this investigation also indicated that $CBXNa_2$ is a versatile dispersing, charging and film forming agent for co-EPD of different materials. However, due to the difference in the surface chemistry and properties of different materials, deposition parameters such as $CBXNa_2$ concentration, voltage and solvent must be optimized for each material. $CBXNa_2$ can be used for EPD of other materials, such as carbon nanotubes. The deposition yield (Supplementary information, Figure S1) was comparable with that obtained using a bile salt such as cholic acid sodium salt as a dispersant and film forming agent [24].

4. Conclusions

The deposition mechanism of pure $CBXH_2$ involved protonation of CBX^{2-} in the anodic reactions and the forming of insoluble $CBXH_2$ films. The EPD mechanism of carbon materials, PTFE and composites involved adsorption of CBX^{2-} on particles, electrophoretic transport and discharge of adsorbed CBX^{2-}, which facilitated film formation. The deposition rate, film morphology and composition can be varied and controlled. $CBXNa_2$ is a versatile surfactant and co-surfactant for EPD of various materials and composites. The EPD method can be applied for protection of metals from corrosion in industry. $CBXNa_2$ is a promising surface modification agent for future applications in EPD of functional inorganic materials due to the chelating properties of its carboxylic groups. Therefore, further progress in $CBXNa_2$ applications can result in the manufacturing of advanced functional composites by EPD.

Supplementary Materials: The following are available online at https://www.mdpi.com/article/10.3390/app11199110/s1, Figure S1: deposition yield measurements and Table S1: Zeta potential measurements

Author Contributions: Conceptualization, X.L., S.V. and I.Z.; methodology, X.L., S.V. and R.M.; validation, X.L.; Formal analysis, X.L. and R.M.; investigation, X.L.; writing—original draft preparation, X.L.; writing—review and editing, X.L. and I.Z.; supervision, I.Z.; project administration, I.Z.; funding acquisition, I.Z. All authors have read and agreed to the published version of the manuscript.

Funding: This research was funded by the Natural Sciences and Engineering Research Council of Canada, grant number RGPIN-2018-04014 and CRC program.

Institutional Review Board Statement: Not Applicable.

Informed Consent Statement: Not Applicable.

Data Availability Statement: The data presented in this study are available in: Carbenoxolone as a multifunctional vehicle for electrodeposition of materials.

Acknowledgments: The authors acknowledge the support of the Natural Sciences and Engineering Research Council (NSERC) of Canada, CRC program and of the Canadian Centre for Electron Microscopy.

Conflicts of Interest: The authors declare no conflict of interest.

References

1. Cheong, M.; Zhitomirsky, I. Electrophoretic deposition of manganese oxide films. *Surf. Eng.* **2009**, *25*, 346–352. [CrossRef]
2. Argüello, J.A.; Cerpa, A.; Moreno, R. Reinforcing effect of graphene nanoplatelets in the electrochemical behaviour of manganese oxide-based supercapacitors produced by EPD. *Ceram. Int.* **2019**, *45*, 14316–14321. [CrossRef]
3. Yus, J.; Bravo, Y.; Sanchez-Herencia, A.J.; Ferrari, B.; Gonzalez, Z. Electrophoretic deposition of RGO-NiO core-shell nanostructures driven by heterocoagulation method with high electrochemical performance. *Electrochim. Acta* **2019**, *308*, 363–372. [CrossRef]
4. Jin, C.; Wang, Y.; Yang, Z.; Wang, D. C/C composite surface modified by electrophoretic depositing SiC nanowires and its brazing to Nb. *Ceram. Int.* **2020**, *46*, 204–211. [CrossRef]
5. Boudaira, R.; Meglali, O.; Bouraiou, A.; Attaf, N.; Sedrati, C.; Aida, M. Optimization of sulphurization temperature for the production of single-phase CZTS kesterite layers synthesized by electrodeposition. *Surf. Eng.* **2020**, *36*, 1000–1011. [CrossRef]
6. Mandal, P.; Mondal, S.C. Enhancement of electro-thermal and mechanical properties for Cu-SWCNT coated 6061Al. *Surf. Eng.* **2020**, *36*, 135–143. [CrossRef]
7. Yang, L.; Pang, X.; Fox-Rabinovich, G.; Veldhuis, S.; Zhitomirsky, I. Electrophoretic deposition of polymer and composite films. *Surf. Eng.* **2012**, *28*, 585–589. [CrossRef]
8. Sun, Y.; Ata, M.; Zhitomirsky, I. Electrophoretic deposition of linear polyethylenimine and composite films. *Surf. Eng.* **2013**, *29*, 495–499. [CrossRef]
9. Jabbari, Z.; Nassernejad, B.; Fallah, N.; Javanbakht, M.; Afsham, N. Fabrication of novel binderless anode via electrophoretic deposition for HT-PEMFC. *Surf. Eng.* **2019**, *35*, 1013–1020. [CrossRef]
10. Emarati, S.M.; Mozammel, M. Fabrication of superhydrophobic titanium dioxide coating on AISI 316L stainless steel by electrophoretic deposition and using trimethoxy (propyl) silane modification. *Surf. Eng.* **2019**, *35*, 456–465. [CrossRef]
11. Rousta, A.; Dorranian, D.; Elahi, M. Electrophoretic deposition of cobalt oxide nanoparticles on aluminium substrate. *Surf. Eng.* **2020**, *36*, 919–928. [CrossRef]
12. Saadati, A.; Hesarikia, H.; Nourani, M.R.; Taheri, R.A. Electrophoretic deposition of hydroxyapatite coating on biodegradable Mg–4Zn–4Sn–0.6 Ca–0.5 Mn alloy. *Surf. Eng.* **2020**, *36*, 908–918. [CrossRef]

13. Gorji, M.; Sanjabi, S.; Edtmaier, C. Combination of electrophoretic and electroless depositions to fabricate Ni/TiC cladding. *Surf. Eng.* **2020**, *36*, 929–935. [CrossRef]
14. Tiwari, P.; Ferson, N.D.; Andrew, J.S. Elucidating the role of electrophoretic mobility for increasing yield in the electrophoretic deposition of nanomaterials. *J. Colloid Interface Sci.* **2020**, *570*, 109–115. [CrossRef] [PubMed]
15. Arguello, J.A.; Rojo, J.M.; Moreno, R. Electrophoretic deposition of manganese oxide and graphene nanoplatelets on graphite paper for the manufacture of supercapacitor electrodes. *Electrochim. Acta* **2019**, *294*, 102–109. [CrossRef]
16. Choudhary, B.; Anwar, S.; Besra, L.; Anwar, S. Electrophoretic deposition studies of Ba (Zr-Ce-Y) O3 ceramic coating. *Int. J. Appl. Ceram. Technol.* **2019**, *16*, 1022–1031. [CrossRef]
17. Jafarpour, M.; Aghajani, H.; Ajabshir, A.G. Stability and electrophoretic deposition of nano-SiC assisted by PEI. *J. Dispers. Sci. Technol.* **2019**, *40*, 1715–1724. [CrossRef]
18. Avcu, E.; Baştan, F.E.; Abdullah, H.Z.; Rehman, M.A.U.; Avcu, Y.Y.; Boccaccini, A.R. Electrophoretic deposition of chitosan-based composite coatings for biomedical applications: A review. *Prog. Mater. Sci.* **2019**, *103*, 69–108. [CrossRef]
19. Sikkema, R.; Baker, K.; Zhitomirsky, I. Electrophoretic deposition of polymers and proteins for biomedical applications. *Adv. Colloid Interface Sci.* **2020**, *284*, 102272. [CrossRef]
20. Deen, I.; Pang, X.; Zhitomirsky, I. Electrophoretic deposition of composite chitosan–halloysite nanotube–hydroxyapatite films. *Colloids Surf. A Physicochem. Eng. Asp.* **2012**, *410*, 38–44. [CrossRef]
21. Amiri, S.; Hayes, R.E.; Sarkar, P. Evolution of electronic conductivity in a Ni/YSZ electrode fabricated by electrophoretic deposition. *Can. J. Chem. Eng.* **2019**, *97*, 1114–1120. [CrossRef]
22. Pang, X.; Zhitomirsky, I.; Niewczas, M. Cathodic electrolytic deposition of zirconia films. *Surf. Coat. Technol.* **2005**, *195*, 138–146. [CrossRef]
23. Zhitomirsky, I.; Petric, A. Electrochemical deposition of yttrium oxide. *J. Mater. Chem.* **2000**, *10*, 1215–1218. [CrossRef]
24. Ata, M.; Zhitomirsky, I. Colloidal methods for the fabrication of carbon nanotube–manganese dioxide and carbon nanotube–polypyrrole composites using bile acids. *J. Colloid Interface Sci.* **2015**, *454*, 27–34. [CrossRef] [PubMed]
25. Ata, M.; Sun, Y.; Li, X.; Zhitomirsky, I. Electrophoretic deposition of graphene, carbon nanotubes and composites using aluminon as charging and film forming agent. *Colloids Surf. A Physicochem. Eng. Asp.* **2012**, *398*, 9–16. [CrossRef]
26. Van der Biest, O.O.; Vandeperre, L.J. Electrophoretic deposition of materials. *Annu. Rev. Mater. Sci.* **1999**, *29*, 327–352. [CrossRef]
27. Ferrari, B.; Moreno, R. EPD kinetics: A review. *J. Eur. Ceram. Soc.* **2010**, *30*, 1069–1078. [CrossRef]
28. Li, J.; Wojtal, P.; Wallar, C.; Zhitomirsky, I. Electrochemical deposition of polypyrrole–carbon nanotube films using steroid dispersants. *Mater. Manuf. Process.* **2018**, *33*, 1062–1066. [CrossRef]
29. Duax, W.; Ghosh, D.; Pletnev, V.; Griffin, J. Three-dimensional structures of steroids and their protein targets. *Pure Appl. Chem.* **1996**, *68*, 1297–1302. [CrossRef]
30. Hou, H.; Banks, C.E.; Jing, M.; Zhang, Y.; Ji, X. Carbon Quantum Dots and Their Derivative 3D Porous Carbon Frameworks for Sodium-Ion Batteries with Ultralong Cycle Life. *Adv. Mater.* **2015**, *27*, 7861–7866. [CrossRef]
31. Ammam, M. Electrophoretic deposition under modulated electric fields: A review. *RSC Adv.* **2012**, *2*, 7633–7646. [CrossRef]
32. Hu, S.; Li, W.; Li, W.; Zhang, N.; Qi, H.; Finklea, H.; Liu, X. Aqueous electrophoretic deposition of gadolinium doped ceria. *Colloids Surf. A Physicochem. Eng. Asp.* **2019**, *579*, 123717. [CrossRef]
33. Sikkema, R.; Keohan, B.; Zhitomirsky, I. Hyaluronic-Acid-Based Organic-Inorganic Composites for Biomedical Applications. *Materials* **2021**, *14*, 4982. [CrossRef] [PubMed]
34. Sikkema, R.; Keohan, B.; Zhitomirsky, I. Alginic Acid Polymer-Hydroxyapatite Composites for Bone Tissue Engineering. *Polymers* **2021**, *13*, 3070. [CrossRef]
35. Zhitomirsky, I.; Gal-Or, L. Formation of hollow fibers by electrophoretic deposition. *Mater. Lett.* **1999**, *38*, 10–17. [CrossRef]
36. Wojtal, P.; Zhitomirsky, I. Surface modification and electrophoretic deposition of materials using 2, 2′-biquinoline-4, 4′-dicarboxylic acid. *Mater. Lett.* **2016**, *174*, 44–47. [CrossRef]
37. Su, Y.; Zhitomirsky, I. Electrophoretic assembly of organic molecules and composites for electrochemical supercapacitors. *J. Colloid Interface Sci.* **2013**, *392*, 247–255. [CrossRef] [PubMed]
38. Cheong, M.; Zhitomirsky, I. Electrodeposition of alginic acid and composite films. *Colloids Surf. A Physicochem. Eng. Asp.* **2008**, *328*, 73–78. [CrossRef]
39. Ata, M.S.; Poon, R.; Syed, A.M.; Milne, J.; Zhitomirsky, I. New developments in non-covalent surface modification, dispersion and electrophoretic deposition of carbon nanotubes. *Carbon* **2018**, *130*, 584–598. [CrossRef]
40. Wang, R.; Xu, G.; He, Y. Structure and properties of polytetrafluoroethylene (PTFE) fibers. *e-Polymers* **2017**, *17*, 215–220. [CrossRef]
41. Ahn, S.; Lee, J.; Kim, H.; Kim, J. A study on the quantitative determination of through-coating porosity in PVD-grown coatings. *Appl. Surf. Sci.* **2004**, *233*, 105–114. [CrossRef]